Tomography of the quantum state of photons entangled in high dimensions

Megan Agnew,[1] Jonathan Leach,[1] Melanie McLaren,[2] F. Stef Roux,[2] and Robert W. Boyd[1,3]

[1]*Department of Physics, University of Ottawa, 150 Louis Pasteur, Ottawa, Ontario, K1N 6N5 Canada*
[2]*CSIR National Laser Centre, Pretoria 0001, South Africa*
[3]*Institute of Optics, University of Rochester, Rochester, New York 14627, USA*

Systems entangled in high dimensions have recently been proposed as important tools for various quantum information protocols, such as multibit quantum key distribution and loophole-free tests of nonlocality. It is therefore important to have precise knowledge of the nature of such entangled quantum states. We tomographically reconstruct the quantum state of the two photons produced by parametric downconversion that are entangled in a d-dimensional orbital angular momentum basis. We determine exactly the density matrix of the entangled two-qu$d$it state with d ranging from 2 to 8. The recording of higher-dimensional states is limited only by the number of data points required and therefore the length of time needed to complete the measurements. We find all the measured states to have fidelities and linear entropies that satisfy the criteria required for a violation of the appropriate high-dimensional Bell inequality. Our results therefore precisely characterize the nature of the entanglement, thus establishing the suitability of such states for applications in quantum information science.

I. INTRODUCTION

Tomographic reconstruction techniques have found applications in a wide range of disciplines. The concept of tomography is that properties of an unknown system that cannot be measured directly are established from a sequence of measurements on different parts of the system. Knowledge about the different measurements and their outcomes are combined to give a best fit to the system that would produce the outcomes of the measurements. An example of tomography in image science is the reconstruction of a three-dimensional object or scene from a number of two-dimensional projections.

Quantum state reconstruction or quantum tomography is the process in which precise knowledge of an unknown quantum state is established [1]. As any measurement on a quantum system will alter the state, the tomographic process requires measurements to be performed on identical copies of the initial state. After a set of measurements is performed, which must form a complete basis in the chosen Hilbert space, the density matrix or quantum state can be uniquely recovered.

The process of reconstruction of a quantum state was proposed by Fano in 1957 [1,2]. Since then, many experiments have been reported, and quantum tomography is an established field of research [3–11]. Recently, quantum tomography using compressive sensing was reported [12]. In that work, it was shown that the number of required measurements to reconstruct the density matrix can be made to scale favorably with the dimension of the quantum system. For specific cases where the density matrix is sparse in a particular basis, there is a significant reduction in the number of measurements required.

We use quantum tomography to reconstruct the state of two entangled photons. Entanglement gives rise to nonclassical correlations of variables in quantum systems; see Ref. [13] for a comprehensive review. These correlations are central to EPR's paradox [14] and tests of nonlocality through violations of Bell inequalities [15,16]. Due in part to its importance for quantum cryptography [17], entanglement has become an important field of study. High-dimensional entanglement

has been reported up to dimension $d = 12$ [18]. The state of hyperentangled photons, which are entangled in several degrees of freedom, has been characterized via quantum state tomography [19]. Tomography of entangled states up to dimension $d = 3$ has also been reported [7]. Higher-dimensionally entangled states have not yet been characterized due to the inherent time demands for the large sets of measurements required.

In this work we determine the precise quantum state of high-dimensionally entangled photon pairs generated by parametric down-conversion. In this process, orbital angular momentum (OAM) is conserved, resulting in two photons with equal but opposite OAMs and entangled in the OAM basis [20–24]. We choose to measure in the OAM basis as the states in this basis are discrete, although the Hilbert space they define is infinite dimensional. It is therefore a simple process to restrict the specific size of the state space while retaining the option of high dimensionality. We see this as an important step in the characterization of high-dimensionally entangled systems, which have recently been proposed as a tool that could be used for loophole-free tests of nonlocality [25].

II. THEORY

The density matrix of a pure quantum state is formed by the outer product of the state vector with itself,

$$\rho = |\psi\rangle\langle\psi|, \tag{1}$$

where the state can be represented in a complete basis of vectors $|u\rangle$ as

$$|\psi\rangle = \sum_u a_u |u\rangle. \tag{2}$$

However, constructing the density matrix from $|\psi\rangle$ requires knowledge of the complex coefficients a_u, which in general cannot be measured directly. This expression also precludes a mixed state, which cannot be expressed with a state vector.

Thus we must use a different approach, such as tomographic reconstruction.

Quantum state tomography consists of reconstructing a density matrix ρ by making multiple measurements on identical copies of the relevant quantum state. The set of measured probabilities p_i for known observables A_i is given by

$$p_i = \text{Tr}[\rho A_i]. \tag{3}$$

Here A_i is a Hermitian operator with real eigenvalues, which in this case is a projection operator composed of the mode that we want to detect. The density matrix is then constructed from a complete set of such measurements. The density matrix must have nonnegative eigenvalues and a trace equal to unity in order to describe a real physical system. It is possible to formulate the calculation of ρ as an inverse problem, where one must invert the matrix A whose rows are composed of the detector states A_i in the basis of the Laguerre-Gauss modes. However, the calculation of ρ using matrix inversion does not always ensure the above conditions due to experimental noise, and different approaches are required to reconstruct physically real quantum states. The method that we use in this paper consists of using linear combinations of generalized Gell-Mann matrices, which form a complete basis set in which to build matrices for any given dimension [6].

In the case of a qubit, a single photon in a two-dimensional state space, the density matrix can be represented as a linear combination of the Pauli matrices [5]. Similarly, the state of a single qu*d*it, which exists in a d-dimensional state space, can be expressed as a linear combination of the generalized Gell-Mann matrices,

$$\rho = \frac{1}{d}\tau_0 + \sum_{n=1}^{d^2-1} b_n \tau_n. \tag{4}$$

Here τ_0 is the d-dimensional identity matrix and τ_n are the generalized Gell-Mann matrices in d dimensions, with corresponding complex coefficients b_n.

This state can also be represented as a superposition of the OAM states of light as

$$|\Psi\rangle = \sum_{\ell=-[d/2]}^{[d/2]} a_\ell |\ell\rangle, \tag{5}$$

where $[x]$ is the integer part of x. We consider only states with mode index $p = 0$. The squares of the coefficients must sum to unity for normalization, and $a_{\ell=0}$ must equal zero for even d. Here, each eigenstate $|\ell\rangle$ denotes a state of light with OAM equal to $\ell\hbar$.

The density matrix of the OAM state of light of Eq. (5) can then be represented by linear combinations of the high-dimensional Gell-Mann matrices as in Eq. (4). The coefficients of these matrices are determined by a set of measurements that must be tomographically complete. One such simple set consists of measurements of the pure OAM states,

$$|\Psi\rangle_\ell = |\ell\rangle, \tag{6}$$

and superpositions of just two of these states,

$$|\Psi\rangle_{\alpha,\ell_1,\ell_2} = \frac{1}{\sqrt{2}}(|\ell_1\rangle + e^{i\alpha}|\ell_2\rangle), \tag{7}$$

where $\ell,\ell_1,\ell_2 = -[d/2],\ldots,[d/2]$ and $\ell_1 < \ell_2$.

In this work, we reconstruct the two-qu*d*it quantum state produced by parametric down-conversion. This process produces two photons with equal and opposite OAMs that are entangled in the OAM basis. The two-photon state is then the tensor product of two single-qu*d*it states from Eq. (5), with opposite OAMs,

$$|\Psi\rangle = \sum_{\ell=-[d/2]}^{[d/2]} c_\ell |\ell\rangle_s \otimes |-\ell\rangle_i. \tag{8}$$

Here, $|c_\ell|^2$ gives the probability of finding a signal photon in state $|\ell\rangle_s$ and idler photon in state $|-\ell\rangle_i$. The range of ℓ over which $|c_\ell|^2$ is appreciable is known as the spiral bandwidth, and detailed analysis of the properties that affect it can be found in Refs. [26–28].

In analogy to using Eq. (4) to represent the single-qu*d*it state of Eq. (5), the density matrix of a two-photon qu*d*it state [Eq. (8)] can be expressed as

$$\rho = \sum_{m,n} b_{m,n} \tau_m \otimes \tau_n, \tag{9}$$

where $b_{0,0} = 1/d^2$ for normalization.

Since we have two qu*d*its, each in a d-dimensional space, we have a state vector of length d^2, resulting in a $d^2 \times d^2$ density matrix. In order to determine the density matrix, we require a number of measurements at least equal to the number of elements in the matrix, which is d^4 [5,7]. These measurements are required to be tomographically complete such that they span the entire state space. A sufficient set would be given by the pure states of Eq. (6) and two superposition states ($\alpha = 0, \frac{\pi}{2}$) from Eq. (7) for each combination of $\ell_1 < \ell_2$ in each of the signal and idler modes of the experiment. For a more accurate reconstruction of the density matrix, one can choose an over-complete set of measurements, thus providing more information with which to reconstruct the state [7].

III. EXPERIMENT

We use parametric down-conversion to generate photon pairs entangled in the transverse degree of freedom. We use a 3-mm-long type I BBO crystal, pumped by a frequency-tripled Nd:YAG laser at 355 nm with an average power of 150 mW and a beam waist of approximately 1 mm (see Fig. 1). In each of the signal and idler arms of the experiment, spatial light modulators (SLMs) together with single-mode fibers act as mode filters which allow us to measure the spatial states of light. In our case, to register a count at the avalanche photodetectors (APDs), light must be converted into the fundamental mode so that it will propagate through the single-mode fibers. This mode conversion is performed by the SLMs, which display computer-generated holograms that convert an incident mode of light depending on the particular phase profile that the SLM represents. The coincidence counting between the two APDs is performed by a National Instruments counting card with a timing resolution of 25 ns.
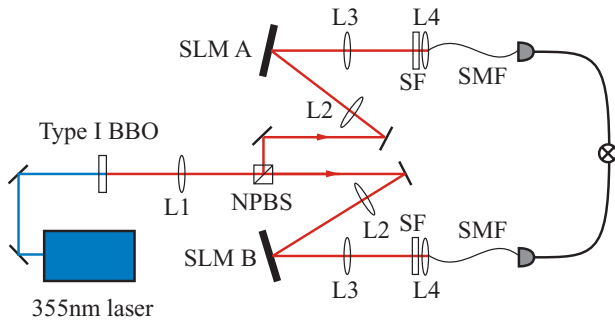
FIG. 1. (Color online) Experimental setup. L1 = 300 mm, L2 = 750 mm, L3 = 1000 mm, L4 = 3.2 mm. SLM, spatial light modulator; NPBS, nonpolarizing beam splitter; SF, 710 ± 5-nm spectral filter; SMF, single-mode fiber.

We take the approach of Ref. [7] by measuring an over-complete set of modes. The range of the signal and idler modes includes all the pure OAM states and all the pure superposition states for all $\ell_1 < \ell_2$; see Eqs. (6) and (7). The phase α between the modes for the superposition states takes on the values $0, \pi/2, \pi$, and $3\pi/2$. The number of possibilities where $\ell_1 < \ell_2$ is equal to the binomial coefficient $\binom{d}{2}$ so that the total number of measurement states for the signal or idler mode is

$$N = 4\binom{d}{2} + d. \tag{10}$$

We measure the coincidence count rates for every combination of these states for both the signal and idler photons, thus resulting in a total number of measurements of N^2. This number increases very quickly with dimension, requiring 225 measurements for $d = 3$ and 14 400 measurements for $d = 8$. For the integration time of 10 s that was used in our experiment, these measurements take approximately 1 and 40 h, respectively.

The measured coincidence count rates are then normalized by dividing all points by the sum of the coincidence counts for the pure OAM states. This converts the coincidence count rates to probabilities so that we can construct a density matrix by minimizing the Chi-square quantity [3,4,11,29],

$$\chi^2 = \sum_{i=1}^{N^2} \frac{\left(p_i^{(M)} - p_i^{(P)}\right)^2}{p_i^{(P)}}. \tag{11}$$

Here, $p_i^{(M)}$ are the measured probabilities from the experiment, and $p_i^{(P)}$ are the predicted probabilities calculated from the guessed density matrix ρ_d, together with the known measurement states A; see Eq. (3).

The reconstruction of a density matrix as given by Eq. (9) does not necessarily have positive eigenvalues and can therefore represent a nonphysical quantum state. Due to the presence of experimental noise, it is in fact likely that such a case occurs. We therefore take an approach to the quantum state reconstruction which ensures that our state has all the required properties.

In order to construct the guessed density matrix ρ_d, we first construct a matrix G from a linear combination of the identity matrix and Gell-Mann matrices for d^2 dimensions. As

these matrices form a basis for any matrix in d^2 dimensions, we ensure a minimum number of coefficients required in the minimization process. The guessed density matrix is then constructed using the following equation, which ensures that all the eigenvalues of ρ_d are positive,

$$\rho_d = \frac{G^\dagger G}{\text{Tr}(G^\dagger G)}. \tag{12}$$

Thus the density matrix is, by construction, Hermitian and positive semidefinite with unit trace [5]. By choosing the appropriate coefficients of the Gell-Mann matrices, we can minimize χ^2, thus producing the closest physical density matrix that represents the high-dimensionally entangled quantum state.

IV. RESULTS AND DISCUSSION

We reconstructed the density matrix of the entangled quantum states for dimensions ranging from $d = 2$ to $d = 8$. The probabilities measured for $d = 5$ are shown in Fig. 2, and reconstructed density matrices for even dimensions are shown in Fig. 3. In each case, the eigenvector with the highest eigenvalue corresponds very closely to the appropriate entangled state given in Eq. (8). The imaginary components
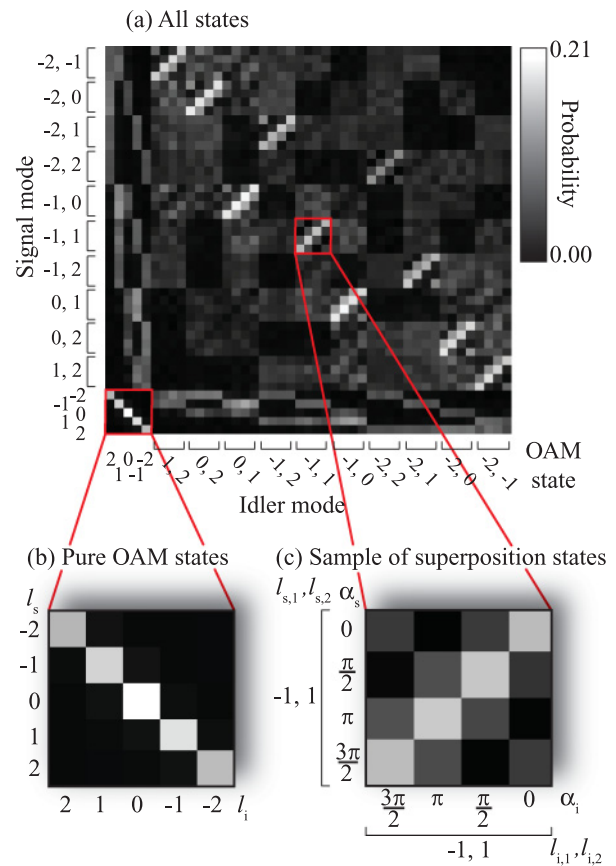

FIG. 2. (Color online) (a) The complete set of measured probabilities for dimension 5. (b) The pure OAM states. (c) A sample of the superposition states. Here, α_i denotes the phase difference in the idler arm, from Eq. (7), and α_s denotes the same in the signal arm. The OAM states separated by a comma denote ℓ_1, ℓ_2 as in Eq. (7), while the single states denote ℓ as in Eq. (6).
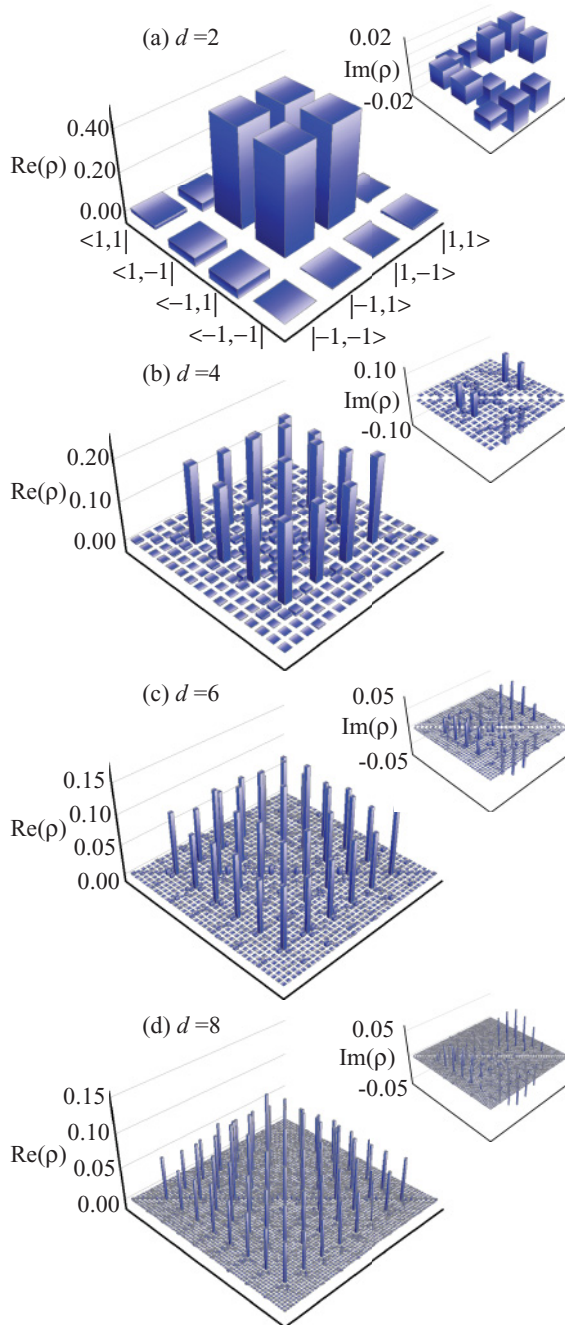
FIG. 3. (Color online) The density matrices for even dimensions 2–8. The axes for dimension 2 are labeled, and the higher dimensions follow the same convention. For example, the labels for the $d = 4$ case would read $\langle 2,2|, \langle 2,1|, \langle 2,-1|, \ldots$ and $|-2,-2\rangle, |-2,-1\rangle, |-2,1\rangle$, etc., where we use the convention $|\ell_s, \ell_i\rangle$ to be equivalent to $|\ell\rangle_s |\ell\rangle_i$.

of the density matrices arise because of coefficients in the entangled states that have a small but measurable phase shift between them. This phase shift occurs because some modes have a larger Gouy phase than others. In our experiment, this phase is detected because the facets of the optical fibers that detect the signal and idler modes may not be in the same optical plane and thus do not image the exact same plane of the nonlinear crystal.
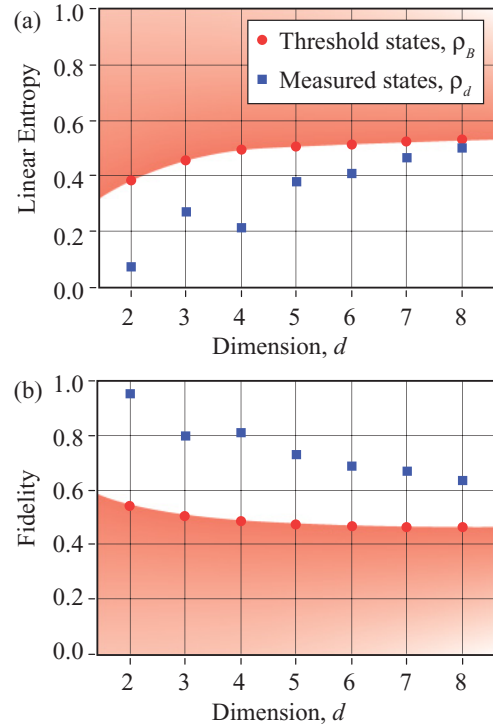

FIG. 4. (Color online) (a) Linear entropy and (b) fidelity as a function of dimension. The error for both of these measurements is ± 0.01, which is too small to be seen clearly on the graphs. In each case, the squares represent the measured data, while the circles represent the threshold states in Eq. (13). The shaded area represents the set of states that will not violate the appropriate high-dimensional Bell inequality.

The density matrix completely characterizes the quantum state; thus once it has been determined, it is simple to make predictions with regards to quantum information protocols. For example, it is possible to determine the degree of entanglement and test whether the states reach the criteria required for violation of the generalized Bell inequalities [16,18].

The linear entropy $S = 1 - \text{Tr}(\rho_d^2)$ is a measure of the purity of the reconstructed state [7]. A pure state has a linear entropy of zero [11]. We find the linear entropy is low for lower dimensions ($S_2 = 0.05 \pm 0.01$), indicating close to pure states. The linear entropy increases with dimension ($S_8 = 0.50 \pm 0.01$), indicating increasingly mixed states [see Fig. 4(a)]. The fidelity is a measure of how close the reconstructed state is to a chosen state and is given by $F = [\text{Tr}(\sqrt{\sqrt{\rho_T} \rho_d \sqrt{\rho_T}})]^2$, where ρ_T is the target density matrix [30]. A perfectly entangled state will have a fidelity of unity with the maximally entangled state in Eq. (8). For low dimensions, we find good fidelity $F_2 = 0.96 \pm 0.01$; however, the fidelity decreases with dimension and becomes as low as $F_8 = 0.64 \pm 0.01$ [see Fig. 4(b)]. The average error for both the entropy and the fidelity is ± 0.01, which is calculated by generating additional data sets by adding $\sqrt{C_i}$ fluctuations to the measured coincidence counts C_i and then repeating the calculations described above.

The generalized Bell inequalities [16,18] test whether or not the observed correlations, which are predicted by quantum mechanics, can be explained by local hidden variable theories.

The quantum state at the threshold of the high-dimensional Bell inequality can be denoted as [16]

$$\rho_B = p_d^{\min}|\psi\rangle\langle\psi| + \left(1 - p_d^{\min}\right)\frac{\mathbb{I}}{d^2}. \tag{13}$$

Here, $\mathbb{I}$ denotes the identity matrix of dimension d^2, and $p_d^{\min}$ is the probability above which the Bell inequality is violated. The linear entropy and fidelity of the state ρ_B for dimensions $d = 2$ through $d = 8$ are shown in Figs. 4(a) and 4(b). A state with a linear entropy below that of ρ_B or a fidelity above that of ρ_B will violate the high-dimensional Bell inequality, and all of our measured states satisfy these conditions.

In the simplest case, the quantum state produced by the parametric down-conversion process is pure [26,27]. Thus the increase in linear entropy with dimension is likely due to errors in the coincidence count rates, which are unavoidable in the detection process. As the required number of measurements increases significantly with the dimension size, so does the possibility for measurement error. The precise origin of the unwanted counts is not clear, although it is recognized that these can arise from accidental coincidences and alignment errors, leading to cross-talk between the modes. Another potential source of error is walk-off, which can lead to spatial distortions of the pump. As far as the fidelity is concerned, since we compare our measured state to the maximally entangled state of Eq. (8) with $c_\ell = 1/\sqrt{d}$, we would expect the measured decrease due to the finite number of entangled modes, which is set by the spiral bandwidth.

The accidental count rate mentioned above can be predicted by taking the product of the single-channel count rates and the coincidence time window. This was less than one count per second for all coincidence measurements. If these predicted accidentals are subtracted from the measured counts, one obtains a more accurate prediction of those that arise solely from the entangled photon pairs. As one would anticipate, repeating the calculations of the density matrices with the background-subtracted data gives rise to quantum states that are purer and have higher fidelities. On average, the fidelity of the background-subtracted data is ≈2% higher than that of the recorded experimental data, while the linear entropy is ≈12% lower. For example, for the background-subtracted data, $S_2 = 0.01$ and $F_2 = 0.98$, while $S_8 = 0.42$ and $F_8 = 0.67$.

V. CONCLUSIONS

We have reported the tomographic reconstruction of the high-dimensional quantum states of photon pairs entangled in the orbital angular momentum basis. We have obtained the density matrix of two entangled qu*d*its in dimensions from $d = 2$ up to $d = 8$. Recording the density matrix of entangled quantum states in higher dimensions is possible, although the required measurement times do not scale favorably with dimension size. Characterizing the states leads to fidelities ranging from $F_2 = 0.96 \pm 0.01$ to $F_8 = 0.64 \pm 0.01$ when compared with the maximally entangled state and linear entropies ranging from $S_2 = 0.05 \pm 0.01$ to $S_8 = 0.50 \pm 0.01$. These measurements and subsequent calculations are important for determining the upper bound on the dimension of an OAM space that is usable for secure quantum communications. It is measurement error that contributes to this increase in entropy and decrease in fidelity. Realizing the extent to which such measurement errors corrupt the state is an important consideration when utilizing such high-dimensionally entangled states in other quantum information protocols.

[1] G. M. D'Ariano, M. G. A. Paris, and M. F. Sacchi, Adv. Imaging Electron Phys. **128**, 205 (2003).

[2] U. Fano, Rev. Mod. Phys. **29**, 74 (1957).

[3] T. Opatrný, D.-G. Welsch, and W. Vogel, Phys. Rev. A **56**, 1788 (1997).

[4] K. Banaszek, G. M. D'Ariano, M. G. A. Paris, and M. F. Sacchi, Phys. Rev. A **61**, 010304 (1999).

[5] D. F. V. James, P. G. Kwiat, W. J. Munro, and A. G. White, Phys. Rev. A **64**, 052312 (2001).

[6] R. T. Thew, K. Nemoto, A. G. White, and W. J. Munro, Phys. Rev. A **66**, 012303 (2002).

[7] N. K. Langford, R. B. Dalton, M. D. Harvey, J. L. O'Brien, G. J. Pryde, A. Gilchrist, S. D. Bartlett, and A. G. White, Phys. Rev. Lett. **93**, 053601 (2004).

[8] G. Molina-Terriza, A. Vaziri, J. Rehacek, Z. Hradil, and A. Zeilinger, Phys. Rev. Lett. **92**, 167903 (2004).

[9] K. J. Resch, P. Walther, and A. Zeilinger, Phys. Rev. Lett. **94**, 070402 (2005).

[10] D. N. Matsukevich, P. Maunz, D. L. Moehring, S. Olmschenk, and C. Monroe, Phys. Rev. Lett. **100**, 150404 (2008).

[11] B. Jack, J. Leach, H. Ritsch, S. M. Barnett, M. J. Padgett, and S. Franke-Arnold, New J. Phys. **11**, 103024 (2009).

[12] A. Shabani, R. L. Kosut, M. Mohseni, H. Rabitz, M. A. Broome, M. P. Almeida, A. Fedrizzi, and A. G. White, Phys. Rev. Lett. **106**, 100401 (2011).

[13] M. D. Reid, P. D. Drummond, W. P. Bowen, E. G. Cavalcanti, P. K. Lam, H. A. Bachor, U. L. Andersen, and G. Leuchs, Rev. Mod. Phys. **81**, 1727 (2009).

[14] A. Einstein, B. Podolsky, and N. Rosen, Phys. Rev. **47**, 777 (1935).

[15] A. Aspect, P. Grangier, and G. Roger, Phys. Rev. Lett. **47**, 460 (1981).

[16] D. Collins, N. Gisin, N. Linden, S. Massar, and S. Popescu, Phys. Rev. Lett. **88**, 040404 (2002).

[17] A. K. Ekert, Phys. Rev. Lett. **67**, 661 (1991).

[18] A. C. Dada, J. Leach, G. S. Buller, M. J. Padgett, and E. Andersson, Nat. Phys. **7**, 677 (2011).

[19] J. T. Barreiro, N. K. Langford, N. A. Peters, and P. G. Kwiat, Phys. Rev. Lett. **95**, 260501 (2005).

[20] H. H. Arnaut and G. A. Barbosa, Phys. Rev. Lett. **85**, 286 (2000).

[21] A. Mair, A. Vaziri, G. Weihs, and A. Zeilinger, Nature (London) **412**, 313 (2001).

[22] S. Franke-Arnold, S. M. Barnett, M. J. Padgett, and L. Allen, Phys. Rev. A **65**, 033823 (2002).

[23] C. I. Osorio, G. Molina-Terriza, and J. P. Torres, Phys. Rev. A **77**, 015810 (2008).

[24] J. Leach, B. Jack, J. Romero, M. Ritsch-Marte, R. W. Boyd, A. K. Jha, S. M. Barnett, S. Franke-Arnold, and M. J. Padgett, Opt. Express **17**, 8287 (2009).

[25] T. Vértesi, S. Pironio, and N. Brunner, Phys. Rev. Lett. **104**, 060401 (2010).

[26] J. P. Torres, A. Alexandrescu, and L. Torner, Phys. Rev. A **68**, 050301 (2003).

[27] F. M. Miatto, A. M. Yao, and S. M. Barnett, Phys. Rev. A **83**, 033816 (2011).

[28] A. M. Yao, New J. Phys. **13**, 053048 (2011).

[29] W. H. Press, S. A. Teukolsky, W. T. Vetterling, and B. P. Flannery, *Numerical Recipes in C* (Cambridge University Press, Cambridge, 2002).

[30] R. Jozsa, J. Mod. Opt. **41**, 2315 (1994).